*molecules*

MDPI

*Article*

# Chemoselective Oxidation of Isoxazolidines with Ruthenium Tetroxide: A Successful Intertwining of Combined Theoretical and Experimental Data

**Laura Legnani [1], Salvatore V. Giofré [2], Daniela Iannazzo [3], Consuelo Celesti [3,4], Lucia Veltri [5] and Maria Assunta Chiacchio [6,*]**

1 Dipartimento di Biotecnologie e Bioscienze, Università di Milano-Bicocca, Piazza della Scienza 2, 20126 Milano, Italy
2 Dipartimento di Scienze Chimiche, Biologiche, Farmaceutiche ed Ambientali, Università di Messina, Viale F. Stagno D'Alcontres, 98166 Messina, Italy
3 Dipartimento di Ingegneria, Università di Messina, Contrada di Dio, 98166 Messina, Italy
4 Dipartimento di Medicina Clinica e Sperimentale, Università di Messina, Via Consolare Valeria, 98125 Messina, Italy
5 Dipartimento di Chimica e Tecnologie Chimiche, Università della Calabria, Via Pietro Bucci 12/C, 87036 Aracavacata di Rende, Italy
6 Dipartimento di Scienze del Farmaco e della Salute, Università di Catania, Viale A. Doria 6, 95125 Catania, Italy
* Correspondence: ma.chiacchio@unict.it

**Abstract:** The direct oxidation reaction of isoxazolidines plays an important role in organic chemistry, leading to the synthesis of biologically active compounds. In this paper, we report a computational mechanistic study of $RuO_4$-catalyzed oxidation of differently *N*-substituted isoxazolidines **1a–c**. Attention was focused on the endo/exo oxidation selectivity. For all the investigated compounds, the exo attack is preferred to the endo one, showing exo percentages growing in parallel with the stability order of transient carbocations found along the reaction pathway. The study has been supported by experimental data that nicely confirm the modeling results.

**Keywords:** ruthenium tetroxide; oxidation; DFT calculations; 3-isoxazolidinone; chemoselectivity



**Citation:** Legnani, L.; Giofré, S.V.; Iannazzo, D.; Celesti, C.; Veltri, L.; Chiacchio, M.A. Chemoselective Oxidation of Isoxazolidines with Ruthenium Tetroxide: A Successful Intertwining of Combined Theoretical and Experimental Data. *Molecules* **2022**, *27*, 5390. https://doi.org/10.3390/molecules27175390

Academic Editors: Marzio Rosi, Stefano Falcinelli and Enrico Bodo

Received: 20 July 2022
Accepted: 22 August 2022
Published: 24 August 2022



## 1. Introduction

Heterocyclic chemistry [1,2] represents one of the most complex and fascinating branches of organic chemistry of equal interest for its theoretical implications [3,4], involving also almost all aspects of modern organic chemistry. The synthesis and functionalization of heterocycles hold a pivotal role in medicinal chemistry, showing a wide range of pharmaceutical and biological properties. Moreover, heterocyclic compounds are key elements in vitamins, hormones, alkaloids, herbicides, dyes, and other products of industrial importance [5–7]. Among the different classes of heterocyclic compounds, some isoxazolidine derivatives, analogs of natural nucleosides and nucleotides, have shown great interest for their anticancer and antiviral properties [8–11]. The synthetic strategies towards these five-membered heterocyclic rings mostly exploited are the classical 1,3-dipolar cycloadditions of nitrones with differently substituted dipolarophiles [12]. The so-formed cycloadducts can be furtherly functionalized to give the 3-isoxazolidinone nucleus, a cyclic Weinreb amide, whose reduction [13] and nucleosidation lead to reverse transcriptase inhibitors [14]. The first example of direct oxidation of isoxazolidines to the 3-isoxazolidinones was reported in the literature in 2007 [15]. This transformation carried out using $RuO_2/NaIO_4$, under ethyl acetate/water biphasic conditions, proved to be highly regioselective, giving only 3-isoxazolidinone derivatives as exclusive compounds.

Based on our expertise in the field of computational mechanistic studies [16,17], we have performed a preliminary study of ruthenium tetroxide-mediated oxidation of

some cyclic and heterocyclic compounds. In these studies, DFT and topological methods highlighted that, on these substrates, the rate-limiting step of the reaction takes place through a highly asynchronous (3 + 2) concerted cycloaddition [18]. More recently, we reported a complete computational mechanistic study concerning the oxidation reaction of 2-methylisoxazolidine with $RuO_4$, taking into consideration the different sites where the oxidation could take place [19]. In fact, all the hydrogen atoms of the isoxazolidine system (C-1′, C-3, C-5, and C-4) could be transferred by oxidation with $RuO_4$ and reactions appeared to be competitive. However, the corresponding barriers for oxidation resulted to be correlated to the stability of the transient carbocation forming along the reaction pathway. So, the *N*-methylisoxazolidin-3-one was detected as the preferred product.

In this paper, with the support of experimental data, we have extended our computational study to isoxazolidines **1a**–**c** (Figure 1), bearing a methyl-carboxylate group at C-5 of the isoxazolidine ring, to avoid competition with oxidation in this position [19]. The results of this study will correlate with the endo/exo oxidation selectivity and follow the carbocations stability order.

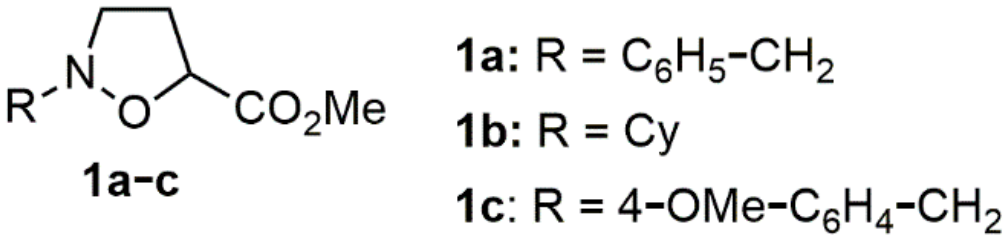


**Figure 1.** *N*-substituted isoxazolidines.

## 2. Results and Discussion

### *2.1. Computational Investigation*

All calculations were performed using the Gaussian16 program package [20]. After a preliminary screening considering different levels of calculation already tested on analogous systems, as reported in the literature [18,19], optimizations were performed using the B3LYP functional [21,22] in conjunction with Grimme's dispersion correction [23,24] (henceforth referred to as B3LYP-d3bj) chosen referring to similar systems' studies [18,19]. The standard basis set Def2SVP was employed [25,26]. Solvent effects water, using the C-PCM method [27,28]) were taken into consideration. As reported [19], the highly asynchronous [3 + 2] one-step oxidation mechanism [29–34] presents two different stages: (a) activation of the R-CH bond, coordinated to the Ru(VI); (b) transfer of the second hydrogen with the obtainment of the oxygenated compound and Ru(IV) (Scheme 1). The first stage is the regioselectivity-determining one and was firstly computationally investigated.

In all the cases, the transition states (**TS1**), leading to **P1** for both the endo and exo pathways (Scheme 1), were located and their 3D plots are reported in Figure 2. For the exo pathway, due to the presence of the stereogenic center at position 5 of the isoxazolidine, and the formation of a second stereogenic center for compounds **1a** and **1c**, the two possible pro-*R* and pro-*S* transition states have been considered. Conversely, for the endo route, it was not possible to locate the pro-*S* transition state, due to the steric hindrance caused by the presence on C-5 of the methylcarboxylate moiety. For the *N*-cyclohexyl derivative **1b**, the two possible $^1C_4$ and $^4C_1$ chair conformations of the six-membered ring, have been examined. The percentages of the compounds derived from the TSs at 298 K, were calculated and the corresponding values are given in Table 1. As expected, contrary to the endo preference detected for the *N*-methylisoxazolidine [19], in all the studied compounds, the exo adduct resulted in being favored by different and, from **1a** to **1c**, growing percentages (63%, 87%, 99%, respectively), related to the stability of the transient carbocation, which is generated during the reaction for the different oxidized compounds.

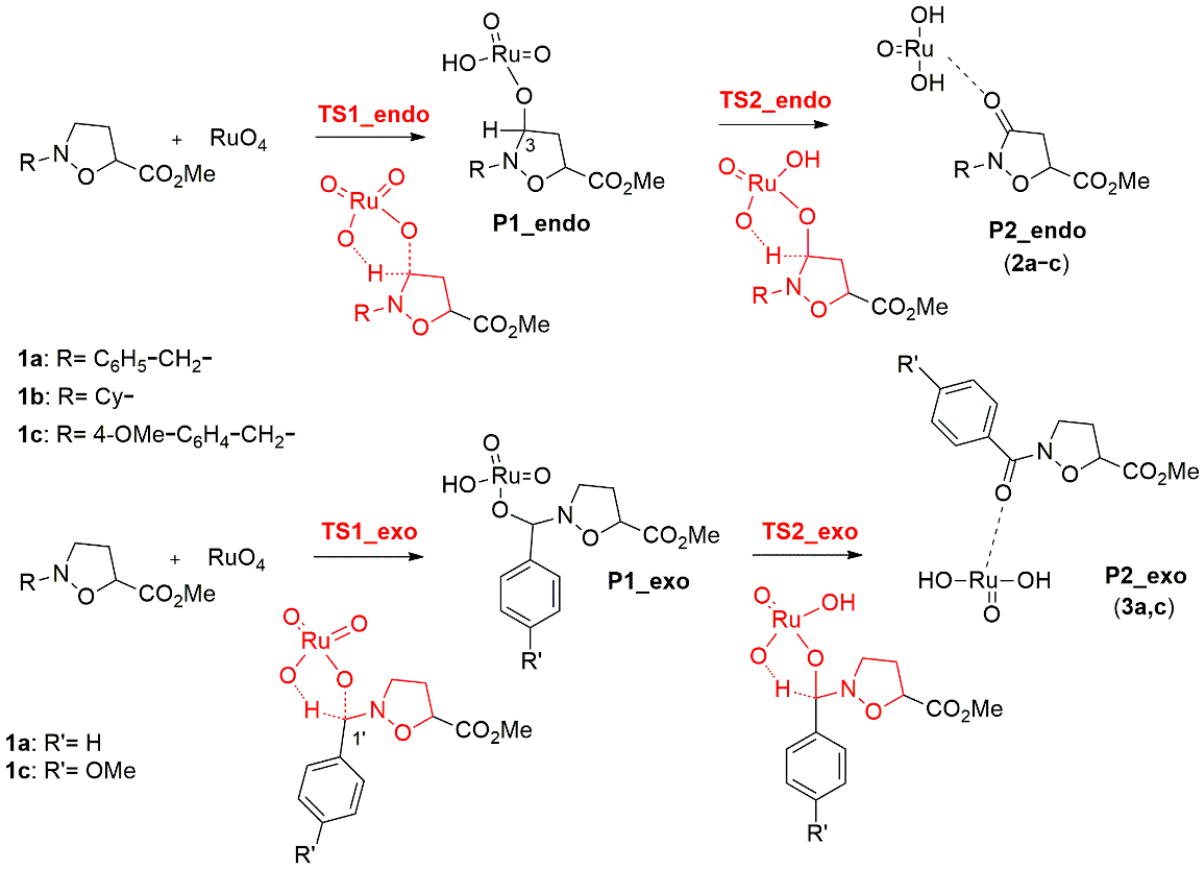


**Scheme 1.** Reaction mechanism of oxidation with $RuO_4$ of compounds **1a–c** in α position to the nitrogen atom.

IRC analyses were performed on all the located **TSs1**. In the case of the forward direction, limited to the exo attack, for **1a–c**, a species very similar to an ion pair [19], with a partial character of the double bond between C-3 and N and the O-Ru-oxygen negative charged, was obtained. Additionally, in this case, for compounds **1a** and **1c**, the two possible diastereomeric routes were investigated. In Figure 3, the three-dimensional plots of representative ion pair structures are reported. The nature of ion pairs IP was confirmed through natural bond order (NBO) analysis (see ESI). When the transfer of the hydrogen atom to the oxygen of the ruthenium occurs, it shows a negative charge (−0.670, −0.694, −0.677 for **1a**, **1b**, and **1c**, respectively), while the corresponding carbon is positively charged (0.205, 0.440 and 0.200 for **1a**, **1b,** and **1c**, respectively). In all ion pairs (IP) large dipole values are detected (IP: 14.3 D; 15.5 D; 15.2 D for **1a**, **1b** and **1c**, respectively). Starting from the ion pair, passing through a very low barrier **TSI** of about 2 kcal/mol (Figure 3), the products **P1** of the first step are obtained. Considering the reaction progression, the second step easily occurred with a new H transfer, with higher barriers (ΔΔG(**TS2**_endo) = 12.88, 18.63, 8.26 kcal/mol, for **1a**, **1b**, and **1c**, respectively, ΔΔG(**TS2**_exo_**proR**) = 23.46, 22.37 kcal/mol; ΔΔG(**TS2**_exo_**proS**) = 12.24, 11.90 kcal/mol for **1a** and **1c**) and so, the second step can be defined as the rate-determining one. For compound **1b**, the second step of reaction takes place only in the endo position since there is no second hydrogen in the exo one. The corresponding three-dimensional plots of transition states **TS2** are reported in Figure 4.

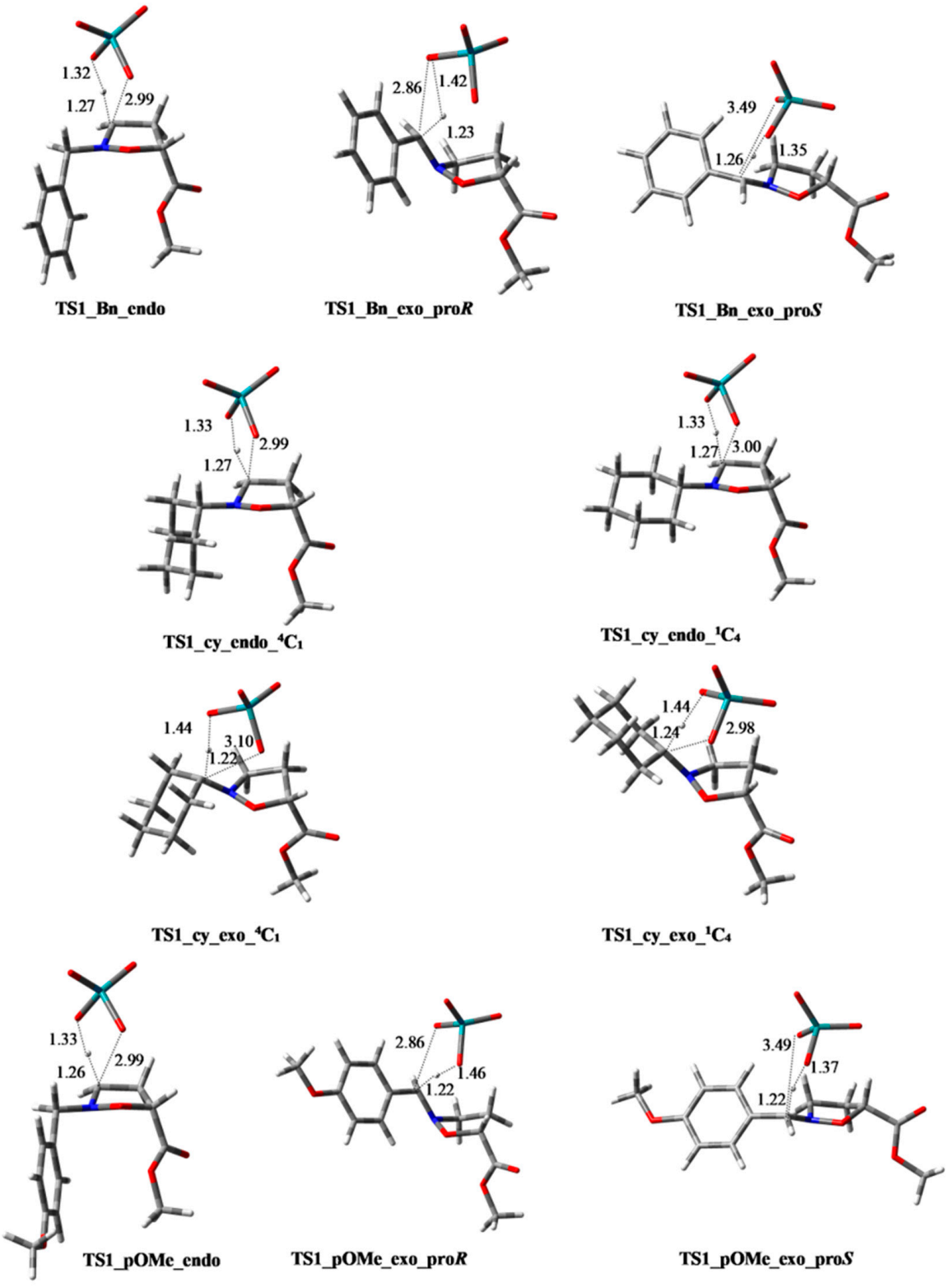


**Figure 2.** Three-dimensional plots of the transition states **TS1** for the endo and exo pathways of compounds **1a**–**c**. Displacement vectors for TS imaginary frequencies are shown as dotted lines and distances are reported in angstroms.

**Table 1.** Relative free energies (kcal/mol) of TSs and percentages of the corresponding products at 298 K of the oxidation reaction with $RuO_4$ of compounds **1a–c**.

| Compounds | | ΔG (kcal/mol) | % | Σ (endo and exo %) |
|---|---|---|---|---|
| **1a** | **TS1_Bn**_endo | 0.00 | 37 | 37 |
| | **TS1_Bn**_exo_**proR** | 0.12 | 31 | 63 |
| | **TS1_Bn**_exo_**proS** | 0.10 | 32 | |
| **1b** | **TS1_cy**_endo_$^4$**C$_1$** | 1.13 | 8 | 13 |
| | **TS1_cy**_endo_$^1$**C$_4$** | 1.42 | 5 | |
| | **TS1_cy**_exo_$^4$**C$_1$** | 0.00 | 52 | 87 |
| | **TS1_cy**_exo_$^1$**C$_4$** | 0.24 | 35 | |
| **1c** | **TS1_pOMe**_endo | 2.32 | 1 | 1 |
| | **TS1_pOMe** _exo_**proR** | 0.00 | 58 | 99 |
| | **TS1_pOMe** _exo_**proS** | 0.21 | 41 | |

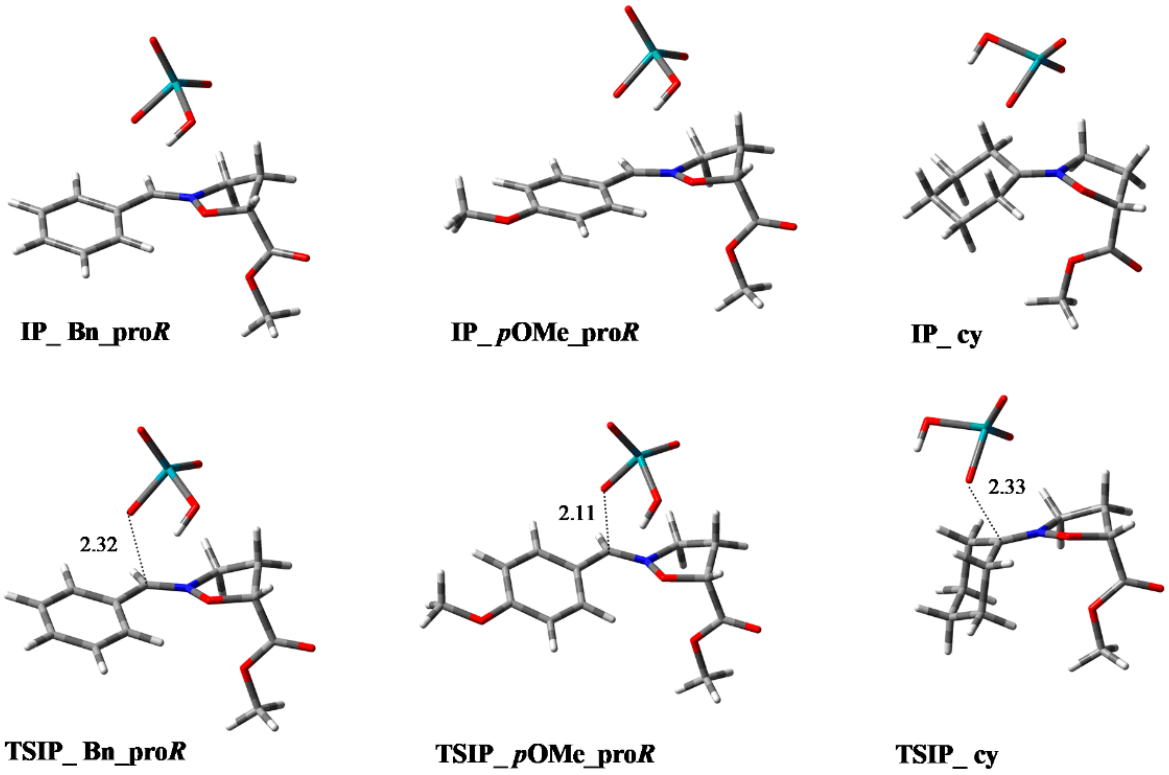


**Figure 3.** Three-dimensional plots of representative conformations of ion pairs (**IP**) and the corresponding transition states (**TSIP**) leading to **P1** for compounds **1a–c**. For TSs imaginary frequencies are shown as dotted lines and distances are reported in angstroms.

When the exo attack occurs on isoxazolidines **1a–c**, the possibility of an alternative route in which a second hydrogen is removed from the endo position, has been evaluated. The obtained products could be the methyl 4,5-dihydroisoxazole-5-carboxylate **4** together with benzaldehyde, cyclohexanone, and 4-metoxybenzaldehyde starting from **1a**, **1b**, and **1c**, respectively (Scheme 2).

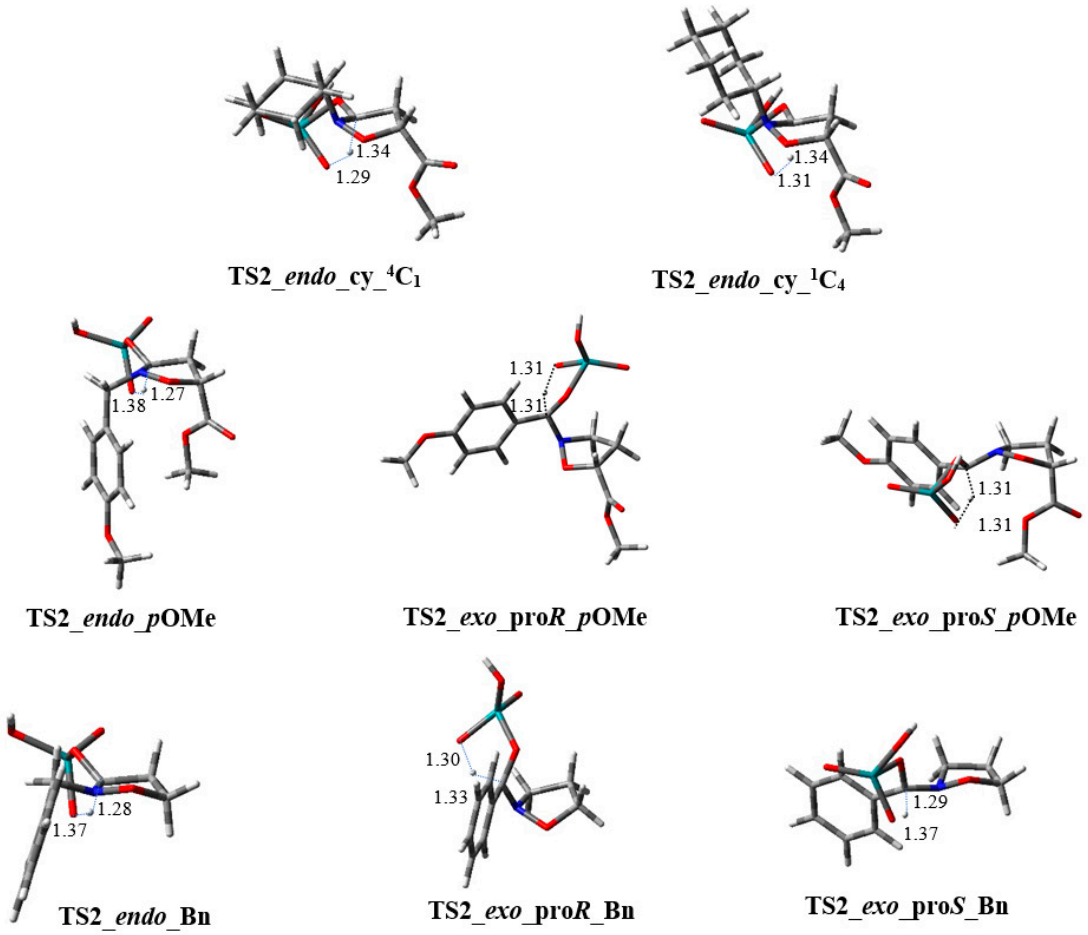


**Figure 4.** Three-dimensional plots of **TS2** leading to **P2** for compounds **1a–c**. For TSs imaginary frequencies are shown as dotted lines and distances are reported in angstroms.

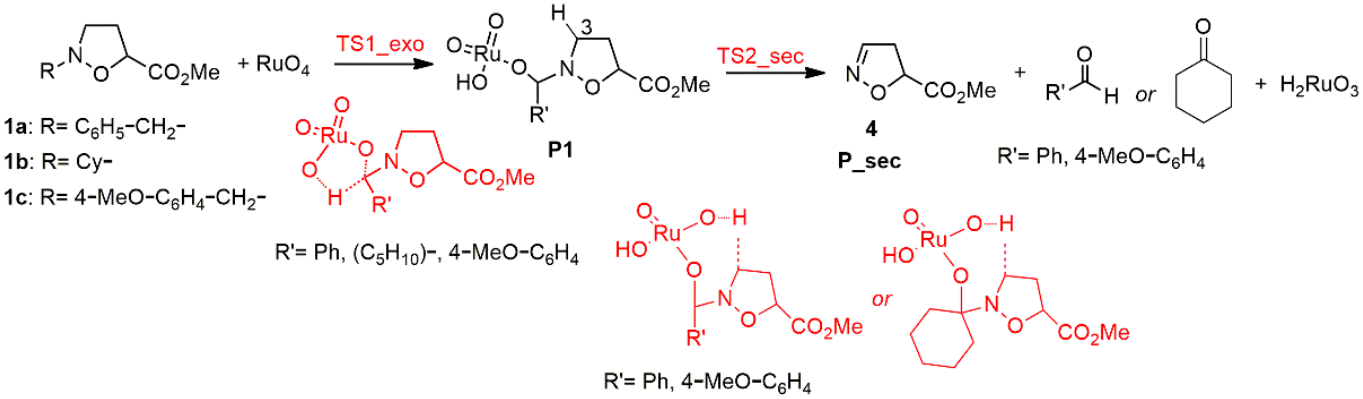


**Scheme 2.** Alternative route for a second H-transfer from the endo position of isoxazolidines **1a–c**.

The corresponding transition states have been located, and the 3D plots of those related to *N*-benzyl **1a** are shown in Figure 5, as an example. However, the corresponding barriers were found to be greater than 25 kcal/mol and therefore this possibility must be excluded.

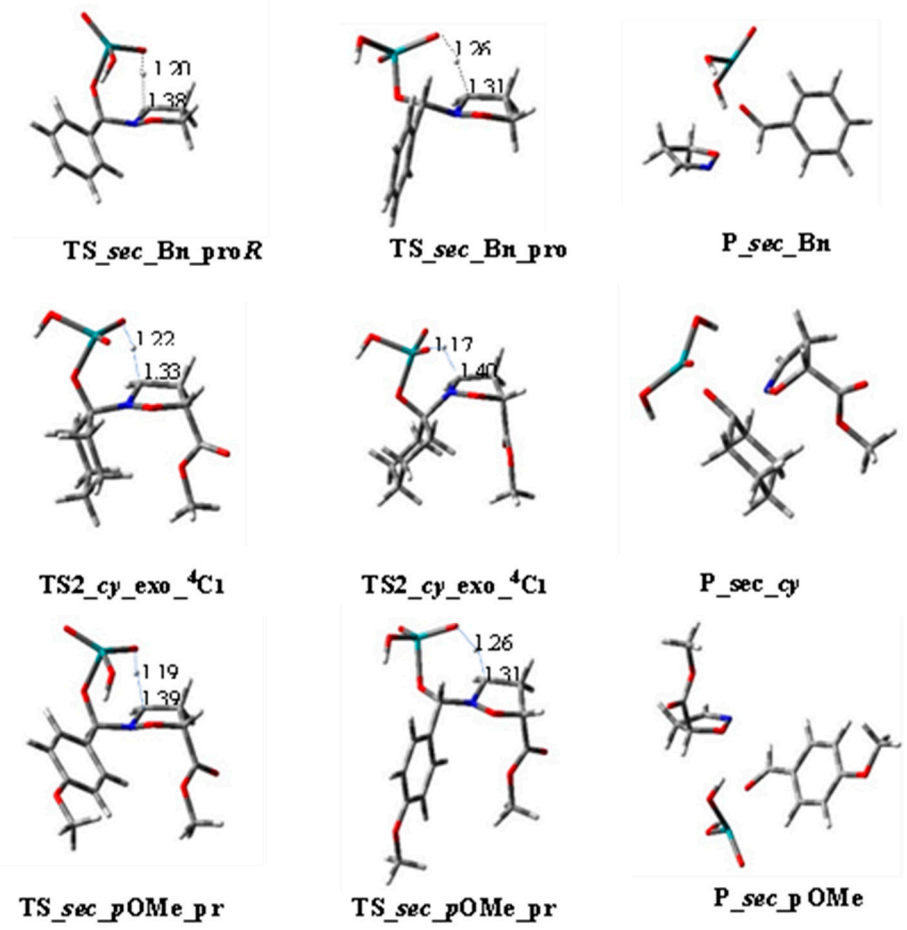


**Figure 5.** Three-dimensional plots of TSs_sec for compounds **1a** and **1c**, **TSs2** for compound **1b,** and the corresponding products **P_sec**. For TSs imaginary frequencies are shown as dotted lines and distances are reported in angstroms.

Moreover, for compound **1b** the second hydrogen transfer can also occur, involving one hydrogen from the β-carbon of the cyclohexyl ring, leading to $H_2$ $RuO_4$ and the corresponding enamine **5** which then evolves to cyclohexanone and methyl-isoxazolidine-5-carboxylate **6** (Scheme 3). However, compound **6** and cyclohexanone could be formed by hydrolysis of **P1**_exo_**cy**.

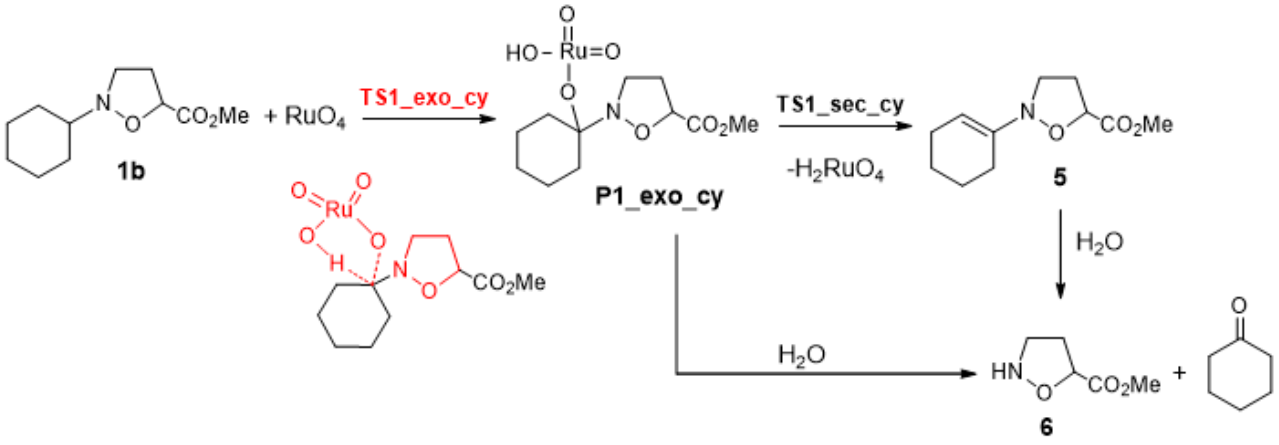


**Scheme 3.** Alternative route for the second H-transfer from β-position of cyclohexyl ring for the exo pathway of **1b**.

We examined this route, considering the possible transfer of both equatorial and axial hydrogens, locating the corresponding transition states. Nevertheless, the calculated barriers are too high (values exceeding 30 kcal/mol) and the reaction, for the second step, cannot proceed through this pathway.

Finally, for compounds **2a–c**, we also explore the possibility of a further attack of $RuO_4$ on **P2-**endo in position exo, considering the two different diastereomeric routes, as shown in Scheme 4. The process is not energetically demanding, with surmountable barriers that make possible the first step of the reaction (ΔΔG(**TS1 b_proR**) = 13.83, 11.87 kcal/mol; ΔΔG(**TS1 b_proS**) = 19.09, 16.17 kcal/mol for **2a** and **2c**, respectively, and ΔΔG(**TS1 b**) = 16.80, 14.34 kcal/mol for **2b** considering conformation $^1C_4$ and $^4C_1$, respectively), that then evolve to **7** and the corresponding carbonyl compounds.

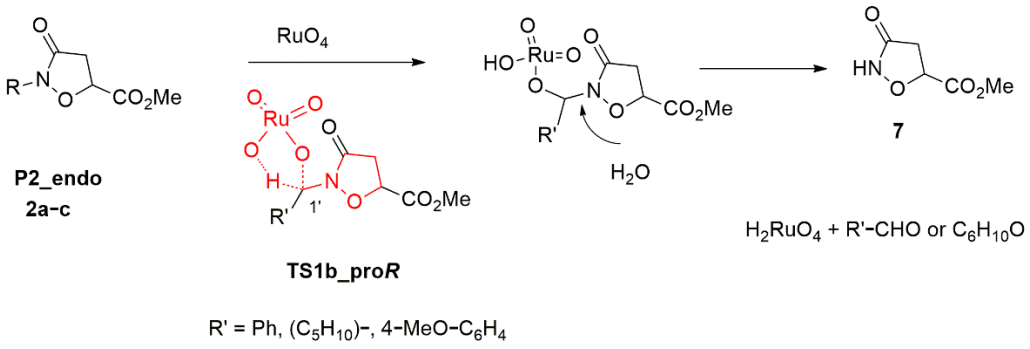


**Scheme 4.** First step of the further oxidation reaction on **P2-**endo (**2a–c**), leading to **7** and corresponding carbonyl compounds.

Once obtained **P1 b-**exo, we also considered the possibility of the second hydrogen extraction at C-1′ with the obtainment of derivatives **8** (Scheme 5). The corresponding calculated barriers are not so high (ΔΔG(**TS2 b**_exo_**proR**) = 19.55, 16.15 kcal/mol; ΔΔG(**TS2 b**_exo_**proS**) = 13.17, 10.80 for **2a** and **2c**) and the oxidation might proceed through the second step. In Figure 6, the 3D plots of the **TSs1 b** of the two steps and the final products **P1 b** obtained at the end of the reaction are reported.

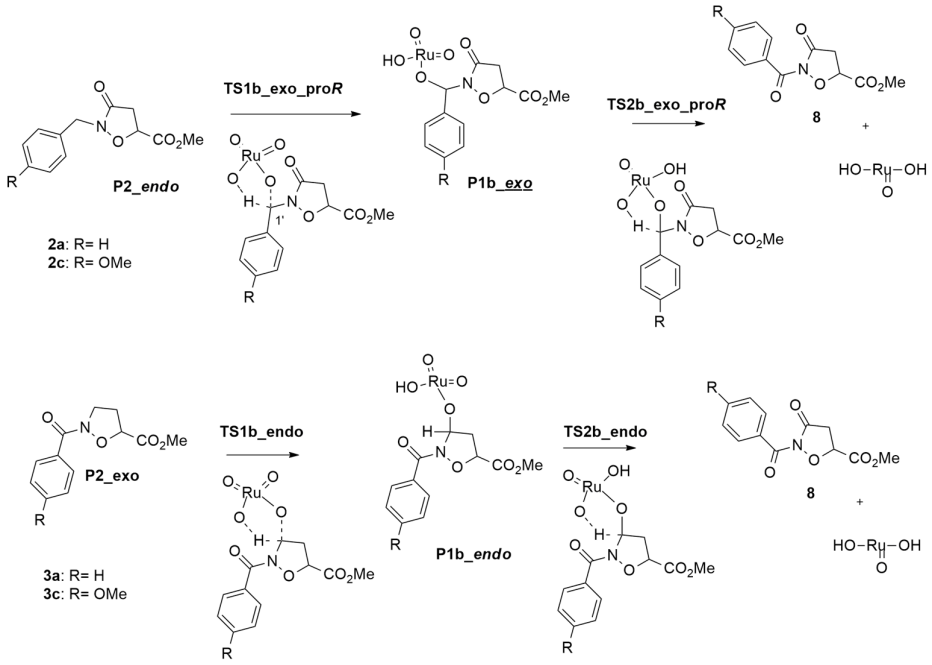


**Scheme 5.** Oxidation reaction on **P2-**endo (**2a**,**c**) and **P2-exo** (**3a**,**c**), leading to **P2 b** (**8**).

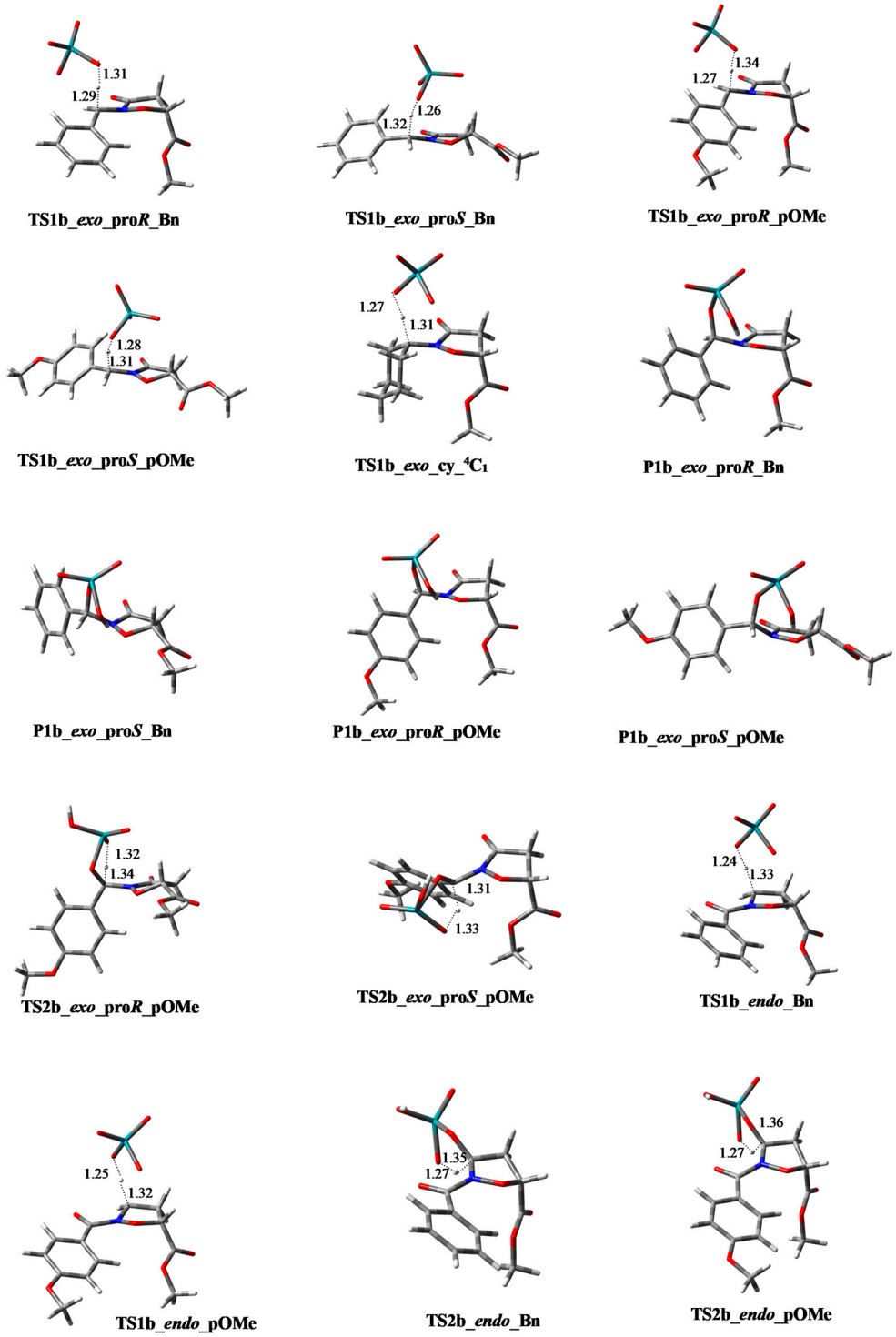


**Figure 6.** Three-dimensional plots of **TSs1–2b** and **P1 b** products. TSs imaginary frequencies are shown as dotted lines and distances are reported in angstroms.

Compound **8** can be also obtained by an oxidation process at the endo position of C-3, starting from **P2**_exo (**3a**,**c**) (Scheme 5). The corresponding calculated barriers are low enough to be surmountable ΔΔG(**TS1 b**_endo) = 17.13, 15.96 kcal/mol; ΔΔG(**TS2 b**_endo) = 21.12, 13.23 for **3a** and **3c**).

IRC analysis in the forward direction for **TS1 b**_exo and **TS1 b**_endo showed a shoulder, corresponding to the ion pair, as determined for the main route. However, when optimized, the ion pairs fell into the energy holes corresponding to **P1 b**_exo and **P1 b**_endo.

### 2.2. Experimental Investigation

To verify the computational outcomes, the first example we have taken into consideration was the oxidation reaction of methyl 2-benzylisoxazolidine-5-carboxylate **1a**. The reaction, using 0.25 equivalent of $RuO_2$ and 1 equivalent of $NaIO_4$, in a biphasic ethyl acetate/water system, occurs in 90 min and provides a mixture of **2a**, **3a**, and **7** in a ratio of 22:60:18, together with a fair amount of benzaldehyde (15% yield) (Scheme 6).

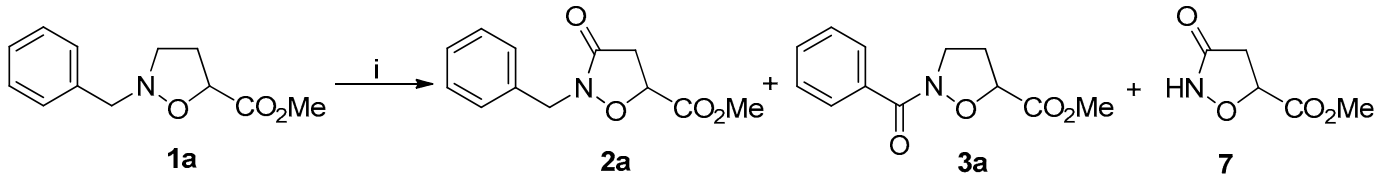


**Scheme 6.** Reagents and conditions: (i) $RuO_2$, $NaIO_4$, ethyl acetate, $H_2$ O, rt., 90 min.

Compound **2a**, according to computational data, can be easily rationalized by an endo attack of $RuO_4$ on the C-3 carbon of the isoxazolidine ring. On the contrary, compound **3a** is formed through a C-1′(exo) attack of $RuO_4$ to the benzylic position of isoxazolidine **1a**. Instead, the methyl 3-oxoisoxazolidine-5-carboxylate **7** derives from the further oxidation reaction of compound **2a** that undergoes a debenzylation process leading also to benzaldehyde (see Schemes 1 and 4). Thus, the oxidation reaction of **1a** proceeds with an exo/endo selectivity of 3:2, showing that this selectivity, according to in silico studies, is controlled by carbocation stability (benzyl vs. secondary carbocation).

Then, following the computational results reported in Table 1, we explored the oxidation reaction of methyl 2-cyclohexyl isoxazolidine-5-carboxylate **1b**, where it is expected that the formation of a tertiary carbocation intermediate is able to increase the exo selectivity. The reaction, performed in the same conditions reported in Scheme 6, gave a mixture of compounds **2b**, **6**, and **7** in a 14:80:6 ratio together with cyclohexanone (Scheme 7). As expected, isoxazolidin-3-one **2b** is produced by an endo attack of $RuO_4$ on **1b** following the route reported in Scheme 1. Compound **6** is probably formed by hydrolysis of **P1**_exo_**cy** (Scheme 3) after exo oxidation of compound **1b**, while compound **7** is produced from **2b** by elimination of cyclohexyl group (Scheme 4). Additionally, for this reaction, the experimental results agree with computational outcomes affording a 4:1 exo/endo selectivity (tertiary vs. secondary carbocation).

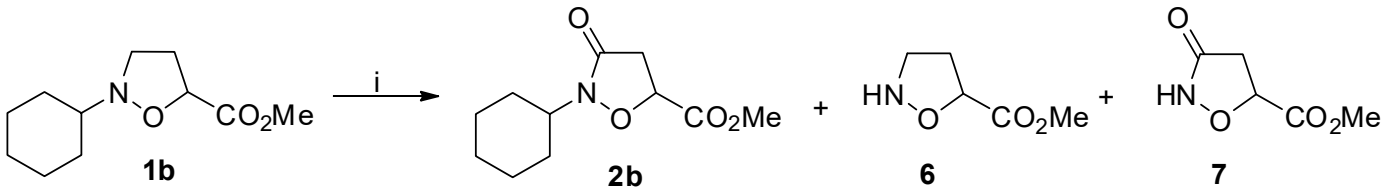


**Scheme 7.** Reagents and conditions: (i) $RuO_2$, $NaIO_4$, ethyl acetate, $H_2$ O, rt, 90 min.

The regioselectivity of $RuO_4$ oxidation favoring the exo attack was also proven on methyl 2-(4-methoxybenzyl) isoxazolidine-5-carboxylate **1c**, which contains an electron donor group in the para position of benzyl group (Scheme 8). The reaction, performed following the same synthetic protocol, afforded compound **3c** in 74.8% yield, 4-methoxybenzaldehyde, and a low amount of **2c** and **7** (5.95% and 4.25 % yield, respectively). The formation of **2c**, **3c**, and **7** are amenable following the routes described in Schemes 1 and 4. For this reaction, the exo/endo ratio was found to be about 9:1, in good agreement with the computational data (4-methoxybenzyl vs. secondary carbocation) (See Supplementary Materials).

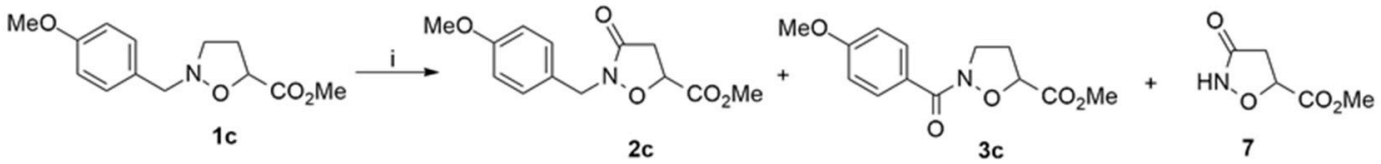


**Scheme 8.** Reagents and conditions: (i) $RuO_2$, $NaIO_4$, ethyl acetate, $H_2$ O, rt, 90 min.

## 3. Materials and Methods

### *3.1. Computational Methods*

All calculations were performed using the Gaussian16 program package [20]. Optimizations were performed using the B3 LYP functional [21,22] in conjunction with Grimme's dispersion correction [23,24] (henceforth referred to as B3 LYP-d3 bj) chosen referring to similar systems' studies [18,19]. The standard basis set Def2 SVP was employed [25,26]. Solvent effects on water, using the C-PCM method [27,28] were taken into consideration. The reaction pathways were confirmed by IRC analyses performed at the same level as above. Vibrational frequencies were computed at the same level of theory to define the optimized structures as minima or transition states, which present an imaginary frequency corresponding to the forming bonds. Thermodynamics at 298.15 K allowed Gibb's free energies to be calculated.

### *3.2. General*

Solvents and reagents were used as received from commercial sources. NMR spectra ($^1$H-NMR recorded at 500 MHz, $^{13}$C-NMR recorded at 125 MHz) were obtained in $CDCl_3$ solution on a Varian instrument (Agilent Technologies, Palo Alto, CA, USA), and data are reported in ppm relative to TMS as an internal standard. Elemental analyses were performed with a Perkin Elmer elemental analyzer (PerkinElmer, Waltham, MA, USA). MW-assisted reactions were performed on a CEM Discover instrument equipped with electromagnetic stirring and an IR probe used for external temperature control (CEM Corporation, NC, USA). Thin-layer chromatographic separations were carried out on Merck silica gel 60-F254 precoated aluminum plates (Merck, Darmstadt, Germany). Preparative separations were carried out using a Büchi C-601 MPLC instrument (BUCHI Italia S.r.l., Milano, Italy) using Merck silica gel 0.040–0.063 mm, and the eluting solvents were delivered by a pump at the flow rate of 3.5–7.0 mL/min. All solvents were dried according to methods in the literature. Isoxazolidines **1a–c** have been synthesized according to standard procedures [8,35].

### *3.3. General Procedure for $RuO_2$/$NaIO_4$ Oxidation*

To a solution of $NaIO_4$ (1 mmol) in water (30 mL) was added $RuO_2$ (0.25 mmol) under nitrogen. The resulting green–yellow solution was stirred for 30 min and was followed by addition of isoxazolidine **1a–c** (0.90 mmol.) in EtOAc (30 mL) in one portion. The solution remained yellowish during the reaction. After 90 min of stirring at room temperature, the mixture was diluted with EtOAc and filtered through a pad of Celite. The organic layer was washed with saturated $NaHSO_3$, which resulted in precipitation of black Ru. The precipitate was filtered off through a pad of Celite. The EtOAc layer was washed with brine and dried with anhydrous $Na_2$ $SO_4$; the solvent was removed by evaporation in a rotary evaporator to obtain the crude product. All products were purified by MPLC chromatography. From **1a** we obtained **2a**, **3a**, and **7** (total yield 85 %), from **1b** we obtained **2b**, **6**, and **7** (total yield 80 %), from **1c** we obtained **2c**, **3c**, and **7** (total yield 85%).

Methyl 2-benzyl-3-oxoisoxazolidine-5-carboxylate (2a): pale yellow oil, yield 18.70%. $^1$H NMR (500 MHz, $CDCl_3$) δ 7.50–7.21 (m, 5 H), 4.86 (dd, J = 9.7, 5.2 Hz, 1 H), 4.76 (d, J = 15.7 Hz, 1 H), 4.67 (d, J = 15.7 Hz, 1 H), 3.72 (s, 3 H), 3.12 (dd, J = 16.8, 9.7 Hz, 1 H), 2.99 (dd, J = 16.8, 5.2 Hz, 1 H) ppm. $^{13}$C NMR (126 MHz, $CDCl_3$) δ 169.57, 167.04, 134.82, 129.21, 128.63, 128.24, 74.29, 52.83, 49.05, 35.89 ppm. Anal. Calcd for $C_{12}H_{13}NO_4$:C, 61.27; H, 5.57; N, 5.95; found C, 61.23; H, 5.55; N, 5.91.

Methyl 2-cyclohexyl-3-oxoisoxazolidine-5-carboxylate (**2b**): yellow oil, 11.20% yield. $^{1}$H NMR (500 MHz, $CDCl_3$) δ 4.83 (t, J = 4.7 Hz, 1 H), 3.82–3.66 (m, 4 H), 3.16–2.95 (m, 2 H), 1.92–1.75 (m, 4 H), 1.66–1.36 (m, 6 H) ppm. $^{13}$C NMR (126 MHz, $CDCl_3$) δ 171.45, 171.11, 73.18, 57.02, 52.37, 36.60, 29.93, 26.25, 24.42. Anal. Calcd for $C_{11}H_{17}NO_4$:C, 58.14; H, 7.54; N, 6.16; found C, 58.15; H, 7.51; N, 6.12.

Methyl 2-(4-methoxybenzyl)-3-oxoisoxazolidine-5-carboxylate (**2c**): pale yellow oil, 5.95% yield. $^{1}$H NMR (500 MHz, $CDCl_3$) δ 7.18 (d, J = 8.6 Hz, 2 H), 6.78 (d, J = 8.6 Hz, 2 H), 4.78 (dd, J = 9.6, 5.2 Hz, 1 H), 4.64 (d, J = 15.5 Hz, 1 H), 4.52 (d, J = 15.5 Hz, 1 H), 3.70 (s, 3 H), 3.65 (s, 3 H), 3.03 (dd, J = 16.8, 9.6 Hz, 1 H), 2.90 (dd, J = 16.7, 5.2 Hz, 1 H) ppm. $^{13}$C NMR (126 MHz, $CDCl_3$) δ 169.83, 169.58, 159.40, 129.68, 126.85, 113.96, 74.22, 55.28, 52.80, 44.36, 35.91 ppm. Anal. Calcd for $C_{13}H_{15}NO_5$:C, 58.86; H, 5.70; N, 5.28; found C, 58.83; H, 5.68; N, 5.25.

Methyl 2-benzoylisoxazolidine-5-carboxylate (**3a**): pale yellow oil, 51%. 1 H NMR (500 MHz, $CDCl_3$) δ 7.85–7.80 (m, 2 H), 7.50–7.44 (m, 1 H), 7.43–7.38 (m, 2 H), 4.68–4.64 (m, 1 H), 4.12–4.03 (m, 1 H), 3.86–3.82 (m, 1 H), 3.64 (s, 3 H), 2.66–2.50 (m, 2 H) ppm. $^{13}$C NMR (126 MHz, $CDCl_3$) δ 170.31, 167.06, 145.39, 133.44, 128.10, 127.94, 77.25, 52.87, 49.09, 31.26 ppm. Anal. Calcd for $C_{12}H_{13}NO_4$:C, 61.27; H, 5.57; N, 5.95; found C, 61.28; H, 5.56; N, 5.94.

Methyl 2-(4-methoxybenzoyl)isoxazolidine-5-carboxylate (**3c**): pale yellow oil, 74.8% yield. $^{1}$H NMR (500 MHz, $CDCl_3$) δ 7.78 (d, J = 8.9 Hz, 2 H), 6.82 (d, J = 8.9 Hz, 2 H), 4.58 (dd, J = 8.5, 4.1 Hz, 1 H), 3.95 (ddd, J = 10.8, 8.7, 7.1 Hz, 1 H), 3.75 (s, 3 H), 3.79–3.71 (m, 1 H), 3.56 (s, 3 H), 2.57–2.39 (m, 2 H) ppm. $^{13}$C NMR (126 MHz, $CDCl_3$) δ 170.78, 170.27, 162.07, 131.34, 125.38, 113.10, 77.14, 55.29, 52.36, 48.41, 31.09 ppm. Anal. Calcd for $C_{13}H_{15}NO_5$:C, 58.86; H, 5.70; N, 5.28; found C, 58.84; H, 5.68; N, 5.29.

Methyl isoxazolidine-5-carboxylate (**6**): white sticky oil, yield 64%. $^{1}$H NMR (500 MHz, $CDCl_3$) δ 4.96 (bs, 1 H), 4.59 (t, J = 3.9 Hz, 1 H), 3.73 (s, 3 H), 3.38–3.26 (m, 1 H), 3.27–3.13 (m, 1 H), 2.23–2.08 (m, 2 H) ppm. $^{13}$C NMR (126 MHz, $CDCl_3$) δ 172.25, 77.32, 52.34, 47.82, 29.52 ppm. Anal. Calcd for $C_5H_9NO_3$:C, 45.80; H, 6.92; N, 10.68; found C, 45.77; H, 6.91; N, 10.62.

Methyl 3-oxoisoxazolidine-5-carboxylate (**7**): white sticky oil (from 1 a, 15.30% yield; from 1 b, 4.8% yield; from 1 c, 4.25% yield). $^{1}$H NMR (500 MHz, $CDCl_3$) δ 8.25 (bs, 1 H), 4.46 (dd, J = 6.1, 5.0 Hz, 1 H), 3.85 (s, 3 H), 2.87 (dd, J = 16.8, 5.0 Hz, 1 H), 2.79 (dd, J = 16.8, 6.1 Hz, 1 H) ppm. $^{13}$C NMR (126 MHz, $CDCl_3$) δ 171.91, 170.32, 66.65, 53.27, 23.39 ppm. Anal. Calcd for $C_5H_7NO_4$:C, 41.38; H, 4.86; N, 9.65; found C, 41.35; H, 4.85; N, 9.66.

## 4. Conclusions

In this paper, we performed a computational mechanistic study of $RuO_4$-catalyzed oxidation of differently *N*-substituted isoxazolidines **1a–c**. Based on our previous results, we first considered the C-3(endo)/C-1′(exo) selectivity, following the supposed [3 + 2] one-step, but asynchronous reaction mechanism with a double hydrogen transfer. In analogy with previously reported results [19], the energy barrier of the second transfer, for compounds **1a** and **1c**, is higher than that of the first one and so the second transfer can be defined as rate-determining. On the other hand, the first one rules the regioselectivity of the reaction and is considered the regioselectivity-determining step.

From the first hydrogen transfer, passing a low energy barrier, **P1**_endo and **P1**_exo are obtained. These intermediates evolve to **2a–c** and **3a**,**c**, after a second hydrogen extraction, resulting in the final compounds oxidized in C-3 or C-1′, respectively. For all compounds **1a–c** the exo attack is preferred to the endo one, showing for the corresponding oxidated product percentages growing from **1a** to **1c**. The computationally determined selectivity in parallel reflects the stability order of transient carbocations involved in the ion pairs. These carbocations were found along the reaction pathway and confirmed by NBO analysis. Once obtained, **P1**_exo can undergo hydrolysis, affording methyl 4,5-dihydroisoxazole-5-carboxylate **4** together with benzaldehyde, cyclohexanone, or 4-methoxybenzaldehyde.

Based on theoretical results, products **2a, c**, and **3a, c** can still react with $RuO_4$, giving a new [3 + 2] one-step process with the obtainment of the dicarbonyl derivative **8**. Nevertheless, the product of the first step **P1 b** can be hydrolyzed before the second oxidation, generating the methyl 3-isoxazolidinone-5-carboxylate **7**.

For the second reaction step, the possibility of hydrogen extraction in alternative positions was examined, but the energy barrier results were too high.

Finally, the computational outcomes have been experimentally confirmed. For all the investigated reactions, the exo attack is preferred to the endo one, confirming that the oxidation selectivity is strictly related to the stability order of transient carbocations found along the reaction pathway.

**Supplementary Materials:** The following are available online at https://www.mdpi.com/article/10.3390/molecules27175390/s1, Figure S1: $^1$H NMR of **2a**; Figure S2: $^{13}$C NMR of **2a**; Figure S3: $^1$H NMR of **2b**; Figure S4: $^{13}$C NMR of **2b**; Figure S5: $^1$H NMR of **2c**; Figure S6: $^{13}$C NMR of **2c**; Figure S7: $^1$H NMR of **3a**; Figure S8: $^{13}$C NMR of **3a**; Figure S9: $^1$H NMR of **3c**; Figure S10: $^{13}$C NMR of **3c**; Figure S11: $^1$H NMR of **6**; Figure S12: $^{13}$C NMR of **6**; Figure S13: $^1$H NMR of **7**; Figure S14: $^{13}$C NMR of **7**; Figure S15: NBO analysis of ion pair IP located along the reaction pathway of compounds **1a**–**c**; B3LYP/def2svp/emp=gd3bj/int=ultrafine/solvent=water cartesian coordinates; Table S1: Free energies and imaginary frequencies for transition states to the oxidation reaction of **1a**; Table S2: Free energies and imaginary frequencies for transition states to the oxidation reaction of **1b**; Table S3: Free energies and imaginary frequencies for transition states to the oxidation reaction of **1b**.

**Author Contributions:** Conceptualization, L.L. and M.A.C.; methodology, L.L., M.A.C., S.V.G., L.V., C.C. and D.I.; software, L.L.; validation, M.A.C.; investigation, S.V.G., L.V. and D.I.; writing—original draft preparation, L.L. and M.A.C.; writing—review and editing, M.A.C. and D.I.; supervision, M.A.C. All authors have read and agreed to the published version of the manuscript.

**Funding:** The authors thank the Universities of Catania (progetto PIACERI 2020–2022 grant number 57722172121), Messina, and Milano-Bicocca for partial financial support.

**Institutional Review Board Statement:** Not applicable.

**Informed Consent Statement:** Not applicable.

**Data Availability Statement:** Not applicable.

**Acknowledgments:** The authors are very grateful to Professor Pedro Merino and Professor Ugo Chiacchio for helpful discussion and to Professor Alessio Porta for providing machine time.

**Conflicts of Interest:** The authors declare no conflict of interest.

## References

1. Nakamura, I.; Yamamoto, Y. Transition-Metal-Catalyzed Reactions in Heterocyclic Synthesis. *Chem. Rev.* **2004**, *104*, 2127–2198. [CrossRef] [PubMed]
2. Scriven, E.; Ramsden, C.A. *Advances in Heterocyclic Chemistry*, 1st ed.; Elsevier Inc.: Amsterdam, The Netherlands, 2021.
3. Ormachea, C.M.; Kneeteman, M.N.; Mancini, P.M.E. Diels–Alder Polar Reactions of Azaheterocycles: A Theoretical and Experimental Study. *Organics* **2022**, *3*, 102–110. [CrossRef]
4. Pappalardo, A.; Ballistreri, F.P.; Toscano, R.M.; Chiacchio, M.A.; Legnani, L.; Grazioso, G.; Veltri, L.; Trusso Sfrazzetto, G. Alkene epoxidations mediated by mn-salen macrocyclic catalysts. *Catalysts* **2021**, *11*, 465. [CrossRef]
5. Jiang, B.; Rajale, T.; Wever, W.; Tu, S.-J.; Li, G. Multicomponent Reactions for the Synthesis of Heterocycles. *Chem. Asian J.* **2010**, *5*, 2318–2335. [CrossRef] [PubMed]
6. Martins, M.A.P.; Frizzo, C.P.; Moreira, D.N.; Buriol, L.; Machado, P. Solvent-Free Heterocyclic Synthesis. *Chem. Rev.* **2009**, *109*, 4140–4182. [CrossRef] [PubMed]
7. Chiacchio, M.A.; Giofrè, S.V.; Romeo, R.; Romeo, G.; Chiacchio, U. Isoxazolidines as biologically active compounds. *Curr. Org. Chem.* **2016**, *13*, 726–749. [CrossRef]
8. Giofrè, S.V.; Romeo, R.; Carnovale, C.; Mancuso, R.; Cirmi, S.; Navarra, M.; Garozzo, A.; Chiacchio, M.A. Synthesis and biological properties of 5-(1H-1,2,3-triazol-4-yl)isoxazolidines: A new class of C-nucleosides. *Molecules* **2015**, *20*, 5260–5275. [CrossRef]
9. Merino, P.; Greco, G.; Tejero, T.; Hurtado-Guerrero, R.; Matute, R.; Chiacchio, U.; Corsaro, A.; Pistarà, V.; Romeo, R. Stereoselective 1,3-dipolar cycloadditions of nitrones derived from amino acids. Asymmetric synthesis of N-(alkoxycarbonylmethyl)-3-hydroxypyrrolidin-2-ones. *Tetrahedron* **2013**, *69*, 9381–9390. [CrossRef]

10. Chiacchio, M.A.; Legnani, L.; Chiacchio, U. Recent Advances in the Synthesis of Isoxazolidines. In *Synthetic Approaches to Nonaromatic Nitrogen Heterocycles*; Phillips, A.M.F., Ed.; John Wiley & Sons Ltd.: Hoboken, NJ, USA, 2020; Volume 1, pp. 161–177.
11. Romeo, G.; Chiacchio, U.; Corsaro, A.; Merino, P. Chemical synthesis of heterocyclic sugar nucleoside analogues. *Chem. Rev.* **2010**, *110*, 3337–3370. [CrossRef]
12. Breugst, M.; Reissig, H.-U. The Huisgen Reaction: Milestones of the 1,3-Dipolar Cycloaddition. *Angew. Chem. Int. Ed.* **2020**, *59*, 12293–12307. [CrossRef]
13. Lanza, G.; Chiacchio, M.A.; Giofrè, S.V.; Romeo, R.; Merino, P. The high selectivity of the $Cp_2$ ZrHCl reducing agent for imides: A combined experimental and theoretical study on γ-lactam and isoxazolidinone derivatives. *Eur. J. Org. Chem.* **2012**, *2013*, 95–104. [CrossRef]
14. Romeo, R.; Giofré, S.V.; Macchi, B.; Balestrieri, M.; Mastino, A.; Merino, P.; Carnovale, C.; Romeo, G.; Chiacchio, U. Truncated Reverse Isoxazolidinyl Nucleosides: A New Class of Allosteric HIV-1 Reverse Transcriptase Inhibitors. *ChemMedChem* **2012**, *7*, 565–569. [CrossRef]
15. Piperno, A.; Chiacchio, U.; Iannazzo, D.; Giofré, S.V.; Romeo, G.; Romeo, R. First Example of Direct $RuO_4$-Catalyzed Oxidation of Isoxazolidines to 3-Isoxazolidones. *J. Org. Chem.* **2007**, *72*, 3958–3960. [CrossRef] [PubMed]
16. Legnani, L.; Puglisi, R.; Pappalardo, A.; Chiacchio, M.A.; Sfrazzetto, G.T. Supramolecular recognition of phosphocholine by an enzyme-like cavitand receptor. *Chem. Commun.* **2020**, *56*, 539–542. [CrossRef] [PubMed]
17. Chiacchio, M.A.; Legnani, L.; Caramella, P.; Tejero, T.; Merino, P. Revealing carbocations in highly asynchronous concerted reactions: The ene-type reaction between dithiocarboxylic acids and alkenes. *Tetrahedron* **2018**, *74*, 5627–5634. [CrossRef]
18. Pedrón, M.; Legnani, L.; Chiacchio, M.A.; Caramella, P.; Tejero, T.; Merino, P. Transient and intermediate carbocations in ruthenium tetroxide oxidation of saturated rings. *Beilstein J. Org. Chem.* **2019**, *15*, 1552–1562. [CrossRef] [PubMed]
19. Chiacchio, M.A.; Iannazzo, D.; Giofré, S.V.; Romeo, R.; Legnani, L. Ruthenium Tetroxide Oxidation of *N*-Methyl-Isoxazolidine: Computational Mechanistic Study. *Arab. J. Chem.* **2022**, *15*, 104063. [CrossRef]
20. *Gaussian 16, Revision C.01*; Gaussian Inc.: Wallingford, CT, USA, 2016.
21. Becke, A.D. Density-functional thermochemistry. III. The role of exact exchange. *J. Chem. Phys.* **1993**, *98*, 5648–5652. [CrossRef]
22. Lee, C.; Yang, W.; Parr, R.G. Development of the Colle-Salvetti correlation-energy formula into a functional of the electron density. *Phys. Rev. B* **1988**, *37*, 785–789. [CrossRef]
23. Grimme, S.; Ehrlich, S.; Goerigk, L. Effect of the damping function in dispersion corrected density functional theory. *J. Comput. Chem.* **2011**, *32*, 1456–1465. [CrossRef]
24. Grimme, S.; Antony, J.; Ehrlich, S.; Krieg, H. A consistent and accurate ab initio parametrization of density functional dispersion correction (DFT-D) for the 94 elements H-Pu. *J. Chem. Phys.* **2010**, *132*, 154104. [CrossRef] [PubMed]
25. Weigend, F. Accurate Coulomb-fitting basis sets for H to Rn. *Phys. Chem. Chem. Phys.* **2006**, *8*, 1057–1065. [CrossRef] [PubMed]
26. Weigend, F.; Ahlrichs, R. Balanced basis sets of split valence, triple zeta valence and quadruple zeta valence quality for H to Rn: Design and assessment of accuracy. *Phys. Chem. Chem. Phys.* **2005**, *7*, 3297–3305. [CrossRef]
27. Barone, V.; Cossi, M.J. Quantum Calculation of Molecular Energies and Energy Gradients in Solution by a Conductor Solvent Model. *Phys. Chem. A* **1998**, *102*, 1995–2001. [CrossRef]
28. Cossi, M.; Rega, N.; Scalmani, G.; Barone, V. Energies, structures, and electronic properties of molecules in solution with the C-PCM solvation model. *J. Comput. Chem.* **2003**, *24*, 669–681. [CrossRef]
29. Mitka, K.; Fela, K.; Olszewska, A.; Jasiński, R. On the Question of Zwitterionic Intermediates in the [3 + 2] Cycloaddition Reactions between C-arylnitrones and Perfluoro 2-Methylpent-2-ene. *Molecules* **2021**, *26*, 7147. [CrossRef]
30. Dresler, E.; Kącka-Zych, A.; Kwiatkowska, M.; Jasiński, R. Regioselectivity, stereoselectivity, and molecular mechanism of [3 + 2] cycloaddition reactions between 2-methyl-1-nitroprop-1-ene and (Z)-C-aryl-N-phenylnitrones: A DFT computational study. *J. Mol. Model.* **2018**, *24*, 329. [CrossRef]
31. Jasiński, R. Competition between one-step and two-step mechanism in polar [3 + 2] cycloadditions of (Z)-C-(3,4,5-trimethoxyphenyl)-N-methyl-nitrone with (Z)-2-EWG-1-bromo-1-nitroethenes. *Comput. Theor. Chem.* **2018**, *1125*, 77–85. [CrossRef]
32. Kącka-Zych, A.; Domingo, L.R.; Jasiński, R. Does a fluorinated Lewis acid catalyst change the molecular mechanism of the decomposition process of nitroethyl carboxylates? *Res. Chem. Intermed.* **2018**, *44*, 325–337. [CrossRef]
33. Kącka-Zych, A.; Domingo, L.R.; Ríos-Gutiérrez, M.; Jasiński, R. Understanding the mechanism of the decomposition reaction of nitroethyl benzoate through the Molecular Electron Density Theory. *Theor. Chem. Acc.* **2017**, *136*, 129. [CrossRef]
34. Kącka, A.B.; Jasiński, R.A. A density functional theory mechanistic study of thermal decomposition reactions of nitroethyl carboxylates: Undermine of "pericyclic" insight. *Heteroat. Chem.* **2016**, *27*, 279–289. [CrossRef]
35. Katahara, S.; Takahashi, T.; Nomura, K.; Uchiyama, M.; Sato, T.; Chida, N. Copper-Catalyzed Electrophilic Etherification of Arylboronic Esters with Isoxazolidines. *Chem. Asian J.* **2020**, *15*, 1869–1872. [CrossRef] [PubMed]